Optical Engineering

OpticalEngineering.SPIEDigitalLibrary.org

Evaluating system penalties in radio frequency photonic links due to photodiode nonlinearity

Nicholas J. Frigo
Meredith N. Hutchinson
Caitlin R. S. Williams

SPIE.

Nicholas J. Frigo, Meredith N. Hutchinson, Caitlin R. S. Williams, "Evaluating system penalties in radio frequency photonic links due to photodiode nonlinearity," *Opt. Eng.* **56**(10), 100501 (2017), doi: 10.1117/1.OE.56.10.100501.

Evaluating system penalties in radio frequency photonic links due to photodiode nonlinearity

Nicholas J. Frigo,[a,b,*] Meredith N. Hutchinson,[a] and Caitlin R. S. Williams[a,c]
[a]U.S. Naval Research Laboratory, Optical Sciences Division, Washington, DC, United States
[b]United States Naval Academy, Physics Department, Annapolis, Maryland, United States
[c]Hastings College, Physics Department, Hastings, Nebraska, United States

Abstract. We extend an earlier second-order characterization of photodiode nonlinearities to third order and present the data as a contour plot over the feasible photodiode operation points. Using this data, we calculate the additional penalty in a nonlinear (i.e., using a Mach–Zehnder modulator) optical link due to the photodiode nonlinearity and illustrate its utility in systems calculations.
© The Authors. Published by SPIE under a Creative Commons Attribution 3.0 Unported License. Distribution or reproduction of this work in whole or in part requires full attribution of the original publication, including its DOI. [DOI: 10.1117/1.OE.56.10.100501]

Keywords: radio frequency/microwave optical links; fiber optics; photodiodes; nonlinearity.

Paper 171146L received Jul. 21, 2017; accepted for publication Sep. 25, 2017; published online Oct. 16, 2017.

1 Introduction

Radio frequency (RF)/microwave photonic links are superior to copper-based links, due to their low-loss and high-bandwidth characteristics.[1] While such characteristics make these links desirable for spectral analysis[2] and communications[3] applications, a potential limitation is the link's linearity: nonlinearities can cause an intermodulation distortion (IMD) that creates "ghost" tones, which masquerade as real signals. As a principal link component, photodiodes have long been studied,[4] and we recently proposed a technique[5] for surveying the system impacts of their nonlinearities.

This survey technique concentrates on the nonlinear impairments created by the photodiode as a function of IMD output frequency, regardless of the input frequencies that contribute to that impairment. As a practical matter, this is how IMD products are manifested in spectral applications,[2] and thus the system impact of these impairments can be observed directly by surveying their effects over the photodiode's feasible operation space. In this letter, we extend our earlier second-order results[5,6] to third-order photodiode nonlinearities and illustrate how to evaluate system penalties they impose. After introducing the experimental setup and our procedure, we present our data, outlining how we obtained a contour plot representation of the system impact of these nonlinearities over the set of feasible operation points. We then discuss the calculation of performance impacts on a system level.

*Address all correspondence to: Nicholas J. Frigo, E-mail: frigo@usna.edu

2 Experimental Characterization

Our setup (Fig. 1) is similar to earlier work.[5,7] Three independent lasers at distinct wavelengths [1547.7 nm (193.7 THz), 1559.8 nm (192.2 THz), and 1550.9 nm (193.2 THz)] are each intensity modulated with RF tones (f_1, f_2, f_3) applied to Mach–Zehnder modulators (MZMs), each stabilized at quadrature. Various physical effects can change optical characteristics[8] over wide wavelength spacing, so our laser wavelengths were chosen as representative of those in an optical link, whereas optical mixing effects were mitigated by frequency spacing (≥500 GHz) that greatly exceed the detection bandwidth. The outputs (individually regulated by variable attenuators) are combined in 3 dB couplers and sent to the photodiode under test. After optical detection by our commercially available 12 GHz pin photodiode, RF signals were recorded with an electrical spectrum analyzer (ESA). To increase dynamic range, we used optical amplifiers (not shown) before the attenuators. We sampled representative system operation points, characterized by (V_{dc}), the bias voltage applied to the diode, and 50-Ω resistor, and the average photocurrent (I_{dc}): these are both accessible system variables. At each operation point, sets of three frequencies were applied to the MZMs, and for each (f_1, f_2, f_3) set, the nonlinear output was logged at each of the four nondegenerate IMD frequencies, represented in Figs. 2 and 3 by: $|f_1 + f_2 + f_3|$ (+), $|f_1 + f_2 - f_3|$ (▶), $|f_1 - f_2 + f_3|$ (◀), and $|f_1 - f_2 - f_3|$ (Δ). We swept f_3 from 30 MHz to 10.11 GHz in steps of 360 MHz for each of the nine choices given by f_1 (2.7, 5.6, and 7.8 GHz) and f_2 (1.1, 4.1, and 9.1 GHz). These sets generate a representative coverage of IMD frequencies: for each (f_1, f_2) pair, each f_3 creates four IMD frequencies, whose symbols are plotted against IMD output frequency (horizontal axis) in Figs. 2 and 3. Thus, each (f_1, f_2) scan consists of 29 different f_3 levels, and each level has up to 4 IMD product symbols in the band. In turn, each operation point has nine such scans.

In a separate experiment, the frequency-dependent RF losses for the system were measured. After the data were collected and corrected for RF losses, each type was sorted by frequency. For each point, we then constructed a dimensionless nonlinear distortion parameter, analogous to the second-order parameter defined earlier,[5,6] by scaling the distortion power to products of the input power

$$\gamma_3(f_{IMD})_{dB} \equiv P(f_{IMD}) - P(f_1) - P(f_2) - P(f_3), \quad (1)$$

where all powers P at the ESA are measured in dBm and $f_{IMD} = |f_1 \pm f_2 \pm f_3|$. A version of this expression is related to the output intercept point OIP3[1,4,7] as we show later.

Figure 2 shows experimental data collected for a single (V_{dc}, I_{dc}) operation point, namely (4 V, 9 mA). The data (all plots in Figs. 2 and 3 have the same horizontal and vertical scales) are plotted as γ_3 in dB against the IMD output

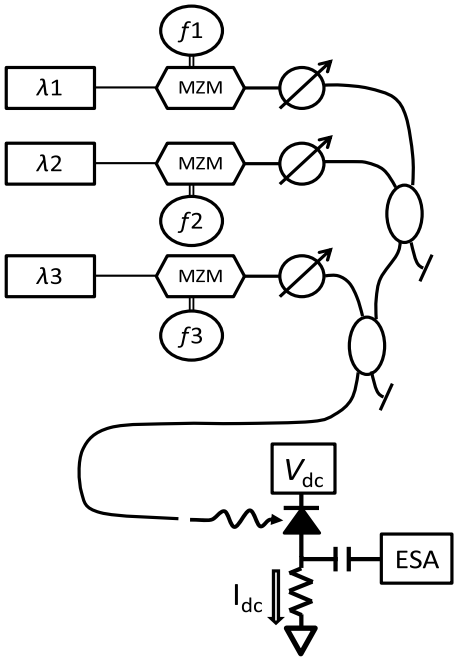

Fig. 1 Experimental setup. Three independent lasers, modulated at distinct RF tones by MZM biased at quadrature, are optically combined at the photodiode under test. Fundamental and IMD output powers are recorded with an ESA.

frequency in GHz. Figure 2(a) shows the data for the choice of $(f_1, f_2) = (5.6, 4.1)$ GHz. As f_3 is scanned, each of the calculated γ_3 values is plotted against the IMD frequency in which it is detected (legend above and in inset). Near each IMD output frequency there are either two or three combinations, as shown by the symbols. This operation point (4 V, 9 mA) has an additional eight combinations of (f_1, f_2). When those nine plots are superimposed into a composite, we obtain the plot in Fig. 2(b), which characterizes this operation point. The maximum γ_3 as a function of frequency (dashed line) varies by 15 dB over the photodiode bandwidth, and it can be used as a detailed specification of nonlinearity. Alternatively, the maximum for this curve over the full bandwidth could be used as a simpler bound for third-order impairments of the photodiode at this operation point.

The data in Fig. 2 represent a single (V_{dc}, I_{dc}) operation point for the photodiode. As in our earlier work,[6] we surveyed the operation points by replicating this experiment

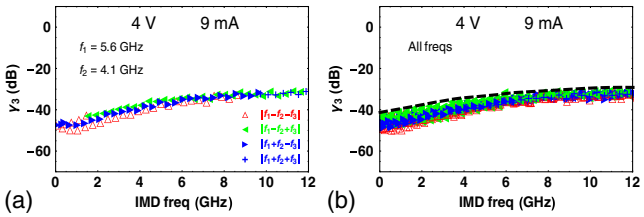

Fig. 2 Plots of γ_3 versus IMD output frequency for a single operation point $V_{dc} = 4$ V, $I_{dc} = 9$ mA. (a) Data for fixed pair $(f_1, f_2) = (5.6\ \text{GHz}, 4.1\ \text{GHz})$ with f_3 ranging from 0.03 to 10.11 GHz. Symbols correspond to differing choices of signs in the IMD products (see text). (b) Composite of plots such as (a) for nine different (f_1, f_2) pairs (see text). The maximum γ_3 as a function of frequency (dashed line) can be used as a specification for third-order frequency-dependent IMD impairment.

over a lattice of (V_{dc}, I_{dc}) operation points, each one comprised of nine scans as in Fig. 2(b). In Fig. 3, the rows (top to bottom) correspond to $I_{dc} = 12, 9, 6$, and 3 mA, whereas the columns (left to right) correspond to $V_{dc} = 2, 4, 6$, and 8 V. The axes and symbols are as in Fig. 2.

Generally speaking, IMD3 for this photodiode is reduced by increasing the bias voltage. Depending on the application and the system sophistication, the data represented in Fig. 3 could be captured either as a set of 16 curves for these operation points, such as the dashed lines in Fig. 2(b) or as the corresponding maxima of these curves. Earlier, we have proposed exploiting similar knowledge of the second-order distortion behavior to reduce IMD2 penalties by "adaptive biasing" of the photodiode during operation.[6]

The data in Fig. 3 can be displayed usefully in a contour plot as shown in Fig. 4. For this plot, we use the same data displayed in Fig. 3 and found the maximum γ_3 for each operation point as a worst-case estimate of the third-order distortion. We generated a numerical interpolation function for these γ_3 maxima using Mathematica, as a function of the (V_{dc}, I_{dc}) operation points. The dots in Fig. 4(a) indicate the location of the operation points used in the interpolation (i.e., the plots shown in Fig. 3). The contours run from −50 (right side, middle) to +10 dB (upper left), in steps of 5 dB and show both a downward sloping penalty with respect to bias voltage and an optimal photocurrent of ∼9 mA. As a check on this contour, we ran an additional series of points at intermediate currents ($I_{dc} = 4.5, 7.5$, and 10.5 mA) for $f_1 = 2.7$ GHz, $f_2 = (1.1, 4.1,$ and 9.1 GHz) and reran the numerical computation. The result, in Fig. 4(b), using the same set of contour levels, shows approximately the same behavior. For comparison, the smaller inset (replicated from Ref. 5) shows that the second-order penalties (γ_2) have distinctly different optimal operation points. The implication of this is that it is not possible to simultaneously optimize the second- and third-order distortion performance for the photodiode: some sort of trade-off must be made at the system engineering level.

3 Discussion

The description of our survey technique assumes a frequency-dependent extension[5] of the simplest model for third-order photodiode nonlinearity, namely $i_{out} = i_{in} + \alpha_3 i_{in}^3$, where i_{in} is the photocurrent observed at a fundamental frequency. We assume a multitone input at the photodetector, $i_{in} = \Sigma_i \phi_i \sin \Omega_i t$, with modulation index $\phi = (\Delta I)/I_{dc}$ used to normalize detected powers to $P_i = \frac{1}{2}\phi_i^2$. Substituting i_{in} into Eq. (1), we find that

$$\gamma_3(\text{dB}) = -20\log_{10}(\text{OIP3}) = 20\log_{10}|3\alpha_3|, \tag{2}$$

for our three-tone experiment. Here, the third-order intercept[1] OIP3, the usual metric for discussing nonlinearities, is that output power for which the extrapolated IMD3 and fundamental powers are equal. This occurs at a normalized amplitude of $\phi = 2$ in our three-tone tests. [We performed three-tone tests to eliminate spurious effects of MZM transmitter nonlinearity, a precaution that is generally unnecessary in RF and microwave tests.[9] For those more conventional two-tone tests,[1,9] the intercept occurs at $\phi = 2\sqrt{2}$. In relating our work to other experiments, OIP3 in Eq. (2) increases by a linear factor of two for two-tone and

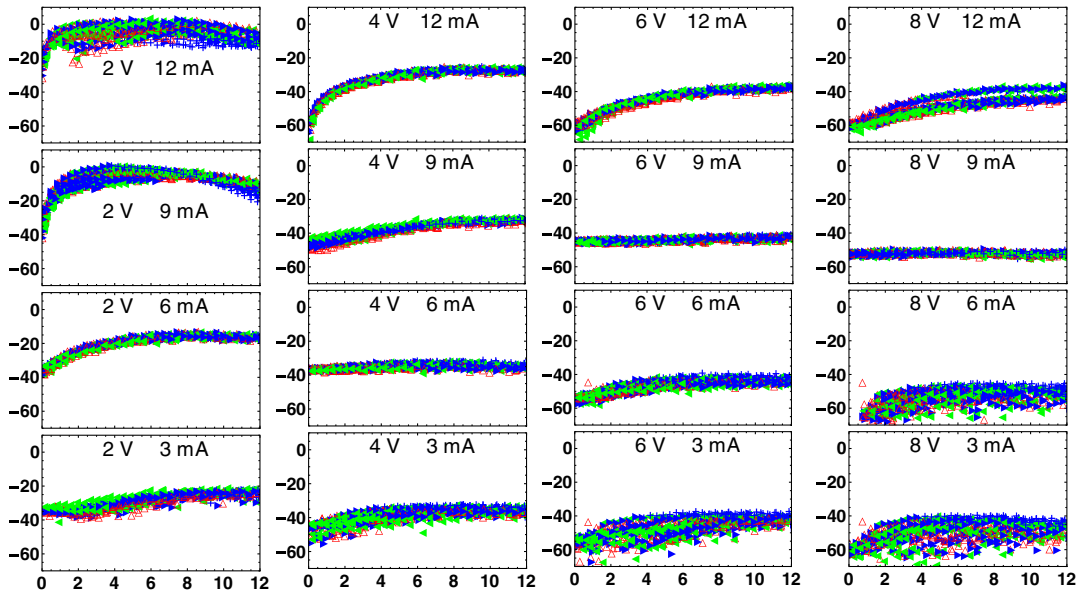

Fig. 3 Plots of composite γ_3 versus IMD output frequency for 16 operation points, each similar to Fig. 2. The rows, top to bottom, correspond to $I_{dc} = 12, 9, 6$, and 3 mA while the columns correspond to $V_{bias} = 2, 4, 6$, and 8 V. Frequency plans and plot axes are as in Fig. 2.

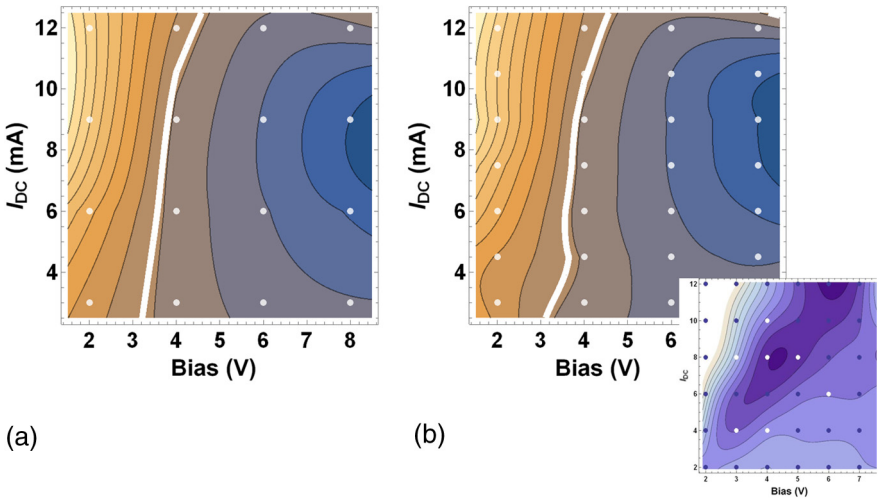

Fig. 4 (a) Contour plots of numerically interpolated γ_3 penalties as in Fig. 3. Contours run from −50 to +10 dB in steps of 5 dB, and represent maximum penalties over photodiode's 12 GHz bandwidth. (b) Contour plot when data from scans with three additional currents are plotted. Contour levels are identical to those in (a). The white curves are operation points for which the photodiode imposes a 0.3 dB penalty for a link with MZM modulator (see Sec. 3). Inset: second-order γ_2 contours from Ref. 6 for comparison.

by six for single-tone experiments, with similar changes in γ_3 for a given nonlinearity α_3.]

This nonlinear formulation can also be applied to the MZM in the transmitter of conventional RF/microwave links.[1] For these transmitters, we have $\alpha_{3,\mathrm{MZM}} = -1/3!$ for the MZM's sinusoidal transfer function. From the system standpoint, the link can be viewed as a cascade[1,9] of two weakly nonlinear subsystems, the transmitter's MZM and the receiver's photodiode, with the result that

$$i_{\mathrm{out}} \approx (i_{\mathrm{in}} + \alpha_{3_{\mathrm{MZM}}} i_{\mathrm{in}}^3) + \alpha_3 (i_{\mathrm{in}} + \alpha_{3_{\mathrm{MZM}}} i_{\mathrm{in}}^3)^3.$$

To lowest order in these weak nonlinearities, this corresponds to an effective third-order nonlinearity of $\alpha_{\mathrm{eff}} \approx \alpha_{3_{\mathrm{MZM}}} + \alpha_3$. Given that the relative phases of these nonlinearities are unknown,[10] it is common practice[9] to assume the worst penalty, which for our three-tone experiment is given by

$$\mathrm{OIP3} = \frac{2}{1 + 6|\alpha_3|}. \tag{3}$$

Since we experimentally determine γ_3, Eq. (2) assigns an experimentally determined α_3 to each point on the $(V_{\mathrm{dc}}, I_{\mathrm{dc}})$ operation space. From this and Eq. (3), we can calculate that, for instance, the photodiode imposes a 0.3-dB additional impairment penalty on the link when $\gamma_3 = -28.9$ dB for

the photodiode. This condition is shown as a white boundary in Fig. 4: points to the right of that curve suffer less than 0.3 dB penalty in third-order distortion due to the presence of the photodiode. As indicated by the distinctly different shapes for the second-order distortion contours in inset of Fig. 4, this presents a "trade space" for system designers to optimize the system performance subject to both nonlinearity orders.

4 Conclusion

We have extended an earlier experimental characterization technique from second- to third-order photodiode nonlinearities, presenting data as a function of IMD output frequency over a wide range of input frequencies. This data was presented as a contour plot of the third-order distortion over a photodiode's useful operation range, and we showed how this could be incorporated into penalty calculations for systems with other known nonlinearities. We illustrated a program by which test engineers can provide systems-level estimates of the nonlinearity penalties due to photodiodes. The process is to:

- characterize the photodiode's performance over the desired operation points as in Fig. 3;
- construct contour functions that describe that performance, as in Fig. 4; and
- use known parameters from other subsystems, calculate penalties or desirable operation spaces using the analysis of Eqs. (2) and (3).

We have shown that the impairments for different orders have different characteristics, which provide a trade-off space for optical engineers to tailor optimization efforts for individual applications.

Acknowledgments

This work was supported in part (NJF) by the Office of US Naval Research (ONR) under Grant No. N0017317WR00205 and in part (CRSW) by the ONR Summer Faculty Research Program.

References

1. V. Urick, J. McKinney, and K. Williams, *Fundamentals of Microwave Photonics*, Wiley, Hoboken, New Jersey (2015).
2. J. Yao, "Microwave photonics," *IEEE J. Lightwave Technol.* **27**(3), 314–335 (2009).
3. R. Ridgway, C. Dohrman, and J. Conway, "Microwave photonics programs at DARPA," *IEEE J. Lightwave Technol.* **32**(20), 3428–3439 (2014).
4. K. Williams, R. Esman, and M. Dagenais, "Nonlinearities in p-i-n microwave photodetectors," *IEEE J. Lightwave Technol.* **14**(1), 84–96 (1996).
5. N. Frigo, M. Hutchinson, and J. Peasant, "Characterization of photodiode nonlinearities by output frequency analysis," *IEEE J. Lightwave Technol.* **34**(20), 4696–4704 (2016).
6. N. Frigo, M. Hutchinson, and C. Williams, "Reduction of photodiode nonlinearity by adaptive bias control," *Electron. Lett.* **53**(3), 175–177 (2017).
7. M. Draa, A. Hastings, and K. Williams, "Comparison of photodiode nonlinearity measurement systems," *Opt. Express* **19**(13), 12635–12645 (2011).
8. Y. Hu et al., "Impact of the Coulomb interaction on the Franz–Keldysh effect in high-current photodetectors," *Opt. Lett.* **41**(3), 456–459 (2016).
9. S. A. Maas, *Nonlinear and Microwave RF Circuits*, 2nd ed., Artech House, Norwood, Massachusetts (2003).
10. Y. Fu et al., "Phase characterization of intermodulation distortion in high-linearity photodiodes," in *Int. Conf. on Indium Phosphide and Related Materials (IPRM)*, pp. 219–220 (2012).